Supporting Information

Insight into Sulfur Rich Selenium Sulfide/Pyrolyzed Polyacrylonitrile Cathodes for Li-S Batteries

Wei Zhang[a], Shuping Li[a], Lihui Wang[a, b], Xumin Wang[a, b], Jia Xie[a*]

[a]State Key Laboratory of Advanced Electromagnetic Engineering and Technology, School of Electrical and Electronic Engineering, Huazhong University of Science and Technology, Wuhan 430074, P. R. China.

[b]State Key Laboratory of Materials Processing and Die & Mould Technology, School of Materials Science and Engineering, Huazhong University of Science and Technology, Wuhan, 430074, China

*Corresponding Author:

Email: xiejia@hust.edu.cn

Table S1. Elemental analysis results of the Se_xS_{1-x}@pPAN composites.

Materials	C (wt%)	N (wt%)	S (wt%)	Se (wt%)	Se_xS_{1-x} (wt%)	S Cap. (based on composites) (mAh g^{-1})	Se Cap. (based on composites) (mAh g^{-1})	Se_xS_{1-x}Cap. (based on composites) (mAh g^{-1})	Se_xS_{1-x}Cap. (based on Se_xS_{1-x}) (mAh g^{-1})
$Se_{0.35}S_{0.65}$@pPAN-350°C	24.73	9.01	27.90	38.04	65.94	467	258	725	1099
$Se_{0.38}S_{0.62}$@pPAN-450°C	32.67	12.11	21.56	33.23	54.79	361	225	586	1071
$Se_{0.44}S_{0.56}$@pPAN-550°C	37.04	13.95	16.48	31.90	48.38	276	216	492	1018
$Se_{0.48}S_{0.52}$@pPAN-650°C	42.36	15.44	12.48	28.99	41.47	209	197	406	978

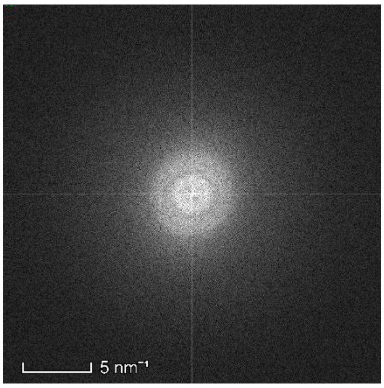

Figure S1. Selected area electron diffraction pattern of the $Se_{0.38}S_{0.62}$@pPAN-450 °C.

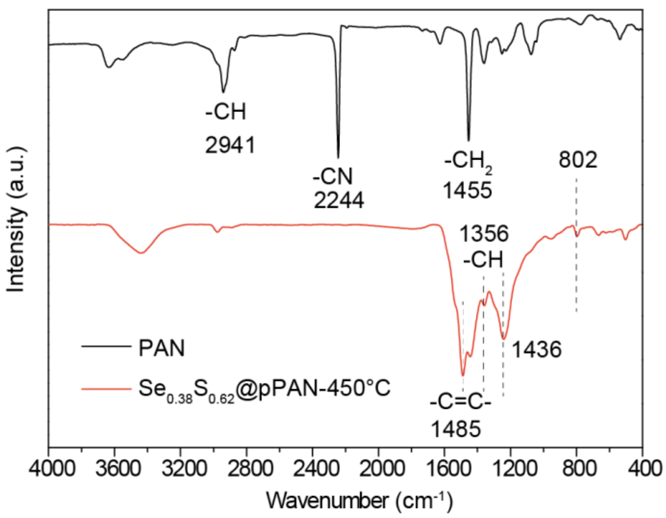

Figure S2. FT-IR spectra of the PAN and $Se_{0.38}S_{0.62}$@pPAN-450 °C.

Table S2. The ratio of I_G/I_D in the Raman spectra for the Se_xS_{1-x}@pPAN composites.

Materials	$Se_{0.35}S_{0.65}$ @pPAN-350°C	$Se_{0.38}S_{0.62}$@ pPAN-450°C	$Se_{0.44}S_{0.56}$@ pPAN-550°C	$Se_{0.48}S_{0.52}$@ pPAN-650°C
I_G/I_D	0.34	0.46	0.51	0.59

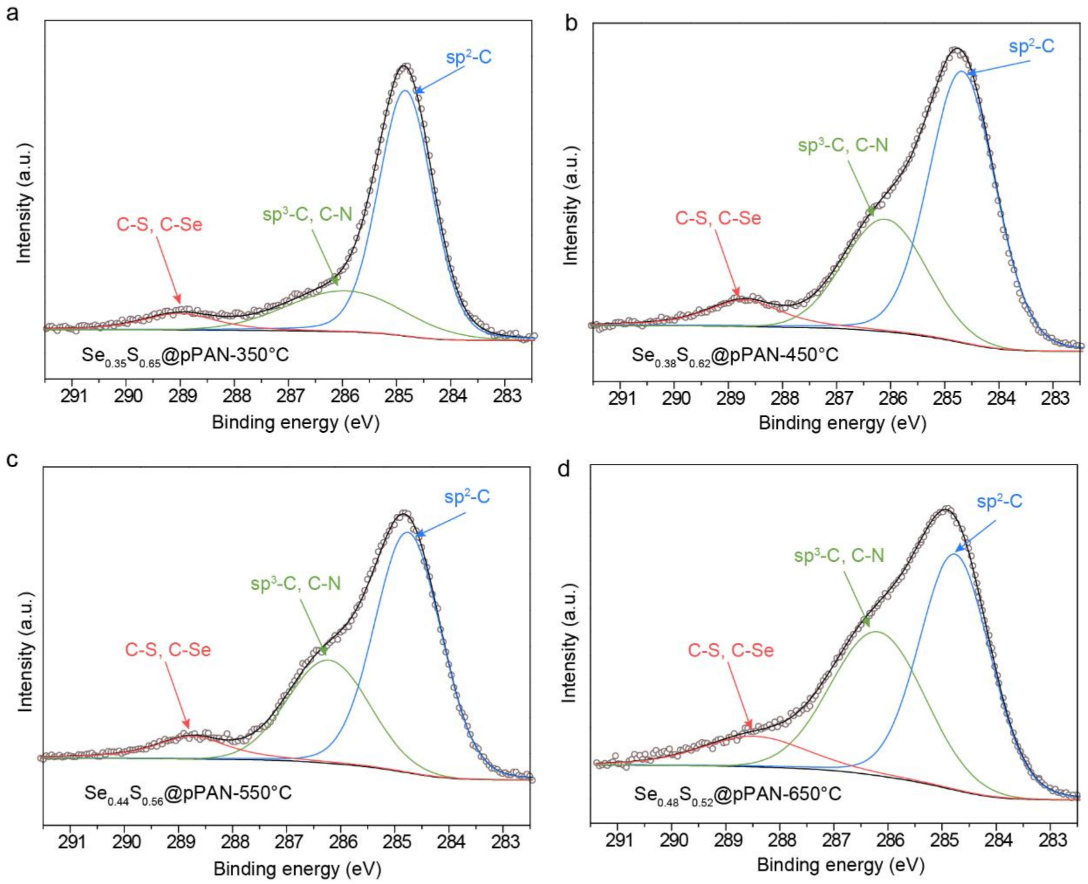

Figure S3. XPS spectra of Se_xS_{1-x}@pPAN composites. C 1s for Se_xS_{1-x}@pPAN.

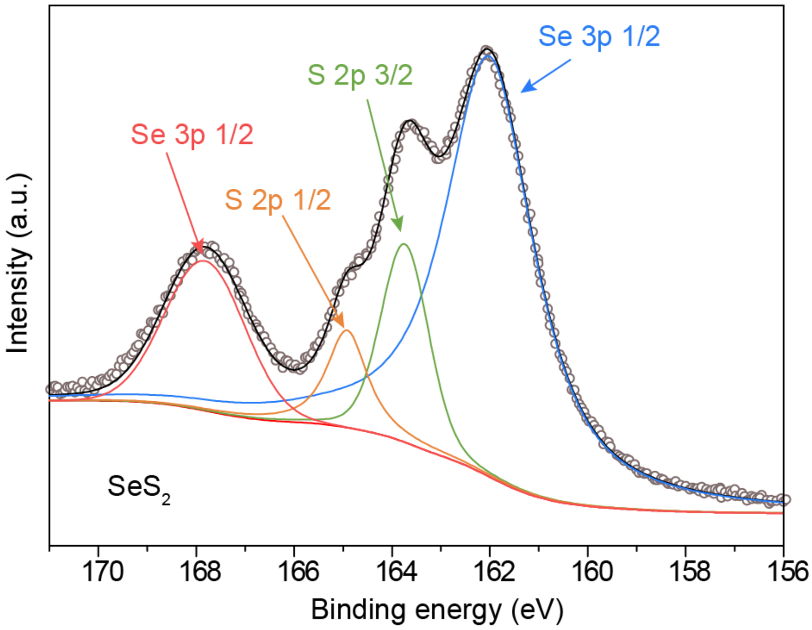

Figure S4. XPS spectra of SeS_2, S 2p and Se 3p

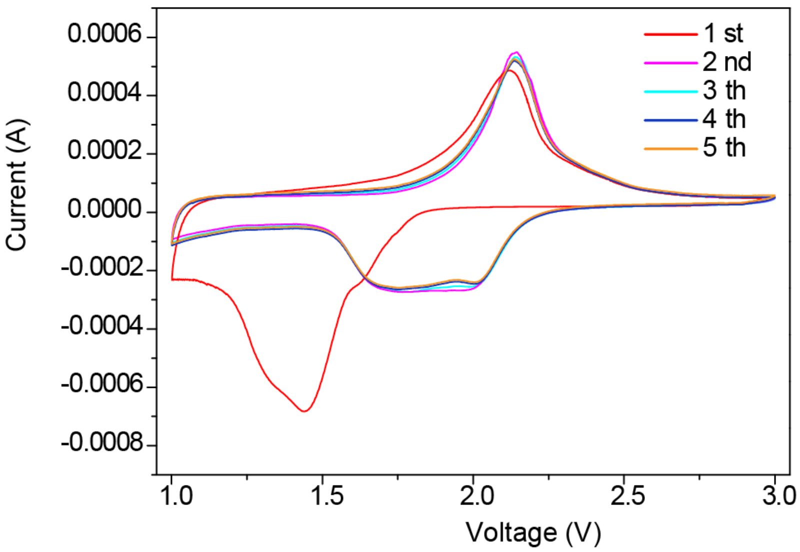

Figure S5. Cyclic voltammograms of the $Se_{0.38}S_{0.62}$@pPAN-450 °C electrode at a scan rate of 0.1 mV/s over a potential window of 1.0-3.0 V (vs. Li^+/Li) in carbonate electrolyte.

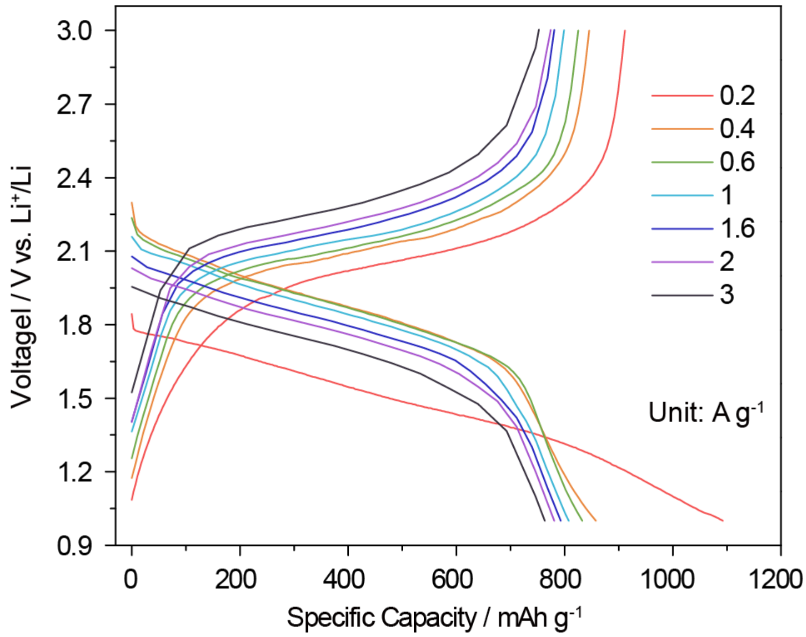

Figure S6. The discharge-charge profiles of the $Se_{0.38}S_{0.62}$@pPAN-450 °C electrode at various current densities from 1.0 to 3.0 V (vs. Li^+/Li) in carbonate electrolyte.

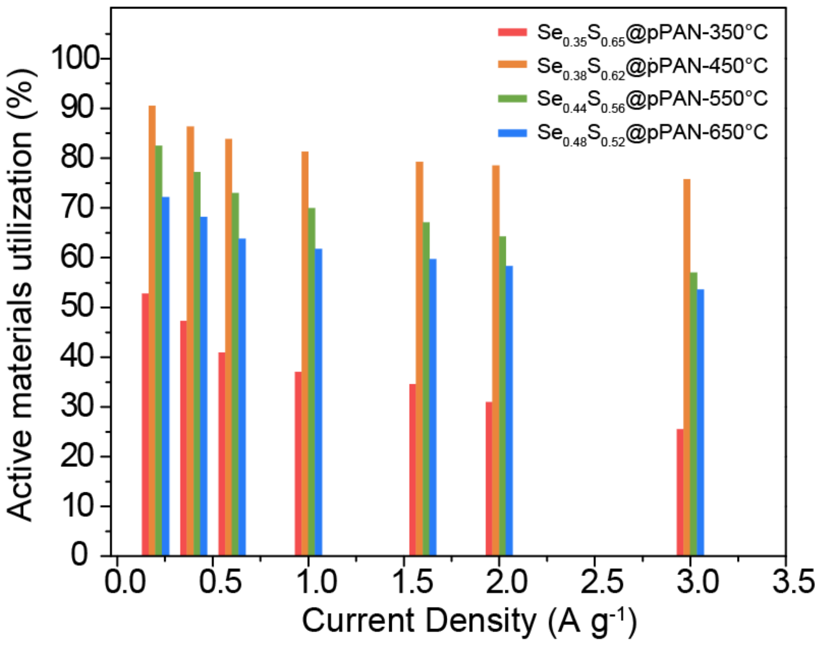

Figure S7. The active material utilization of Se_xS_{1-x}@pPAN electrodes at various current density in carbonate electrolyte.

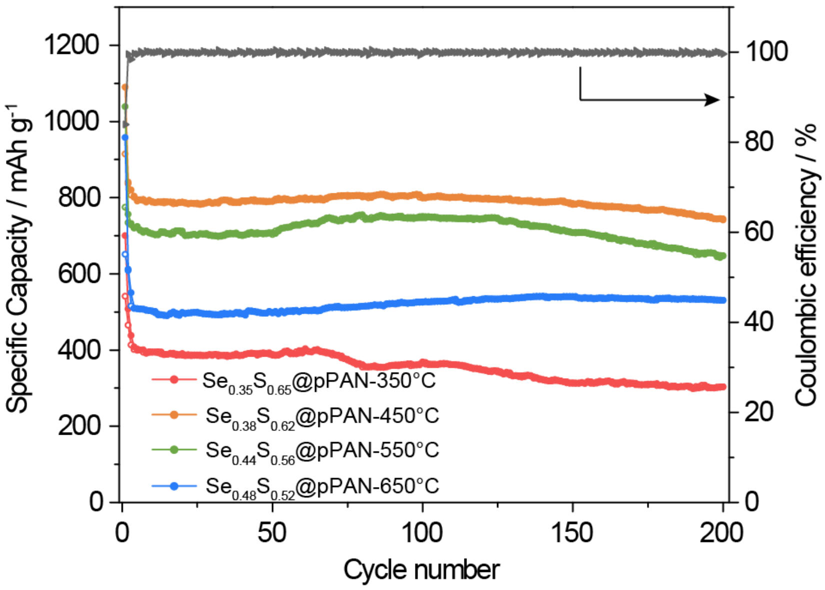

Figure S8. Cycling performances of the Se_xS_{1-x}@pPAN electrodes at 1 A g^{-1} in ether electrolyte.

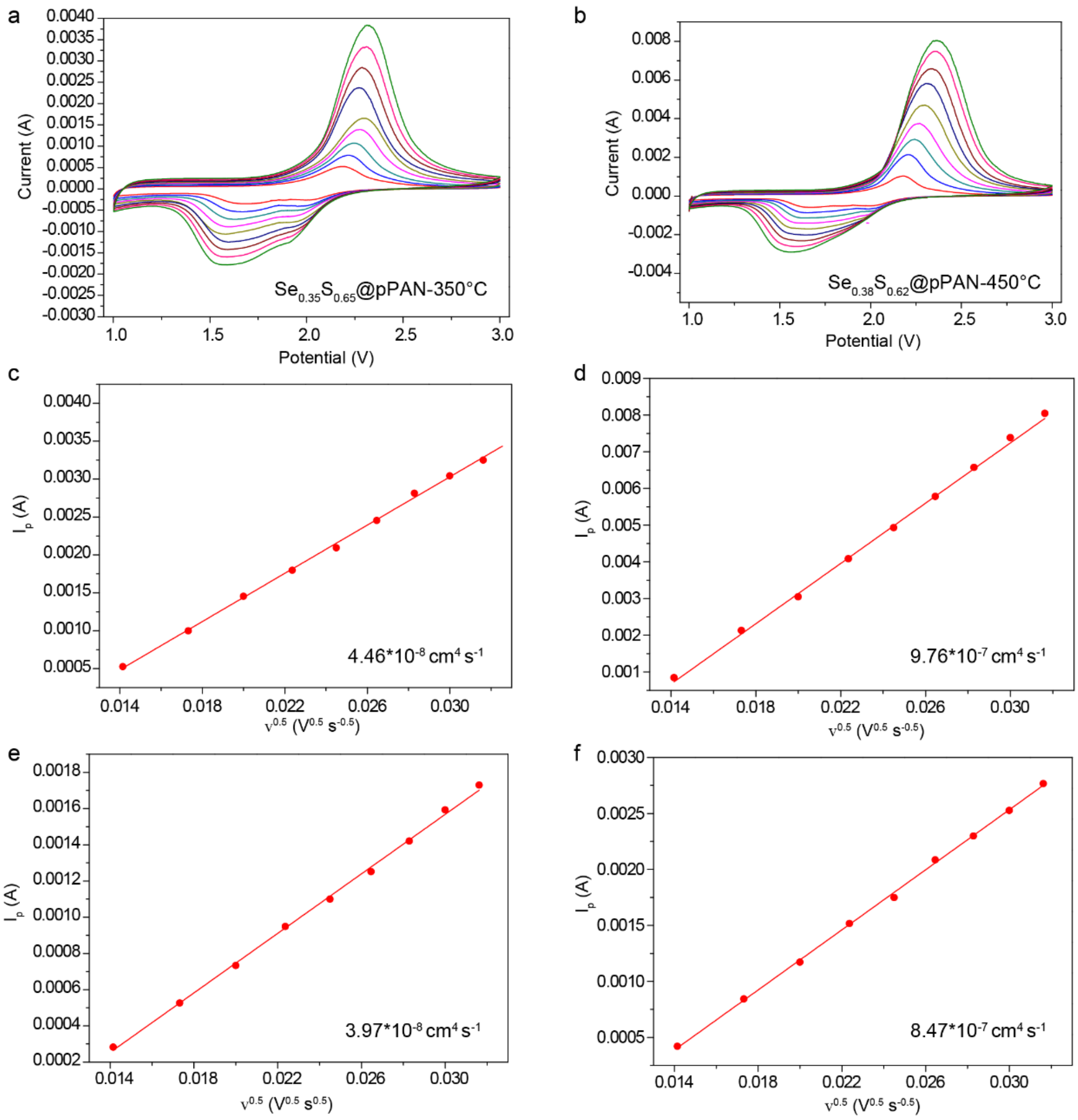

Figure S9. CV curves and peak currents versus square root of scan rates of Se_xS_{1-x}@pPAN electrodes in carbonate electrolyte. (a), (c) and (e) are for $Se_{0.35}S_{0.65}$@pPAN-350 °C; and (b), (d) and (f) are for $Se_{0.38}S_{0.62}$@pPAN-450 °C.

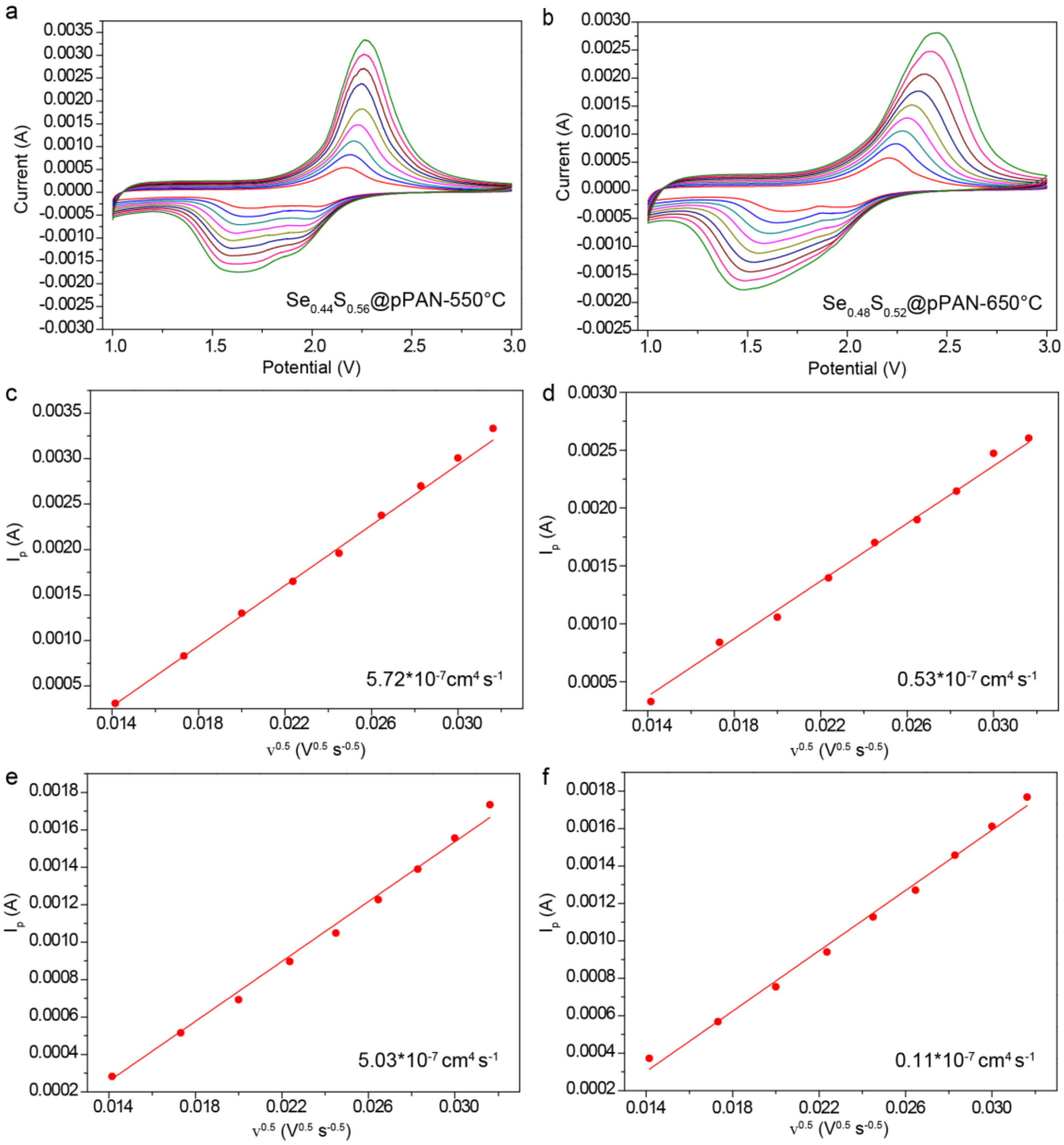

Figure S10. CV curves and peak currents versus square root of scan rates of SeS_2@pPAN electrodes in carbonate electrolyte. (a), (c) and (e) are for $Se_{0.44}S_{0.56}$@pPAN-550 °C; and (b), (d) and (f) are for $Se_{0.48}S_{0.52}$@pPAN-650 °C.

Table S3. Comparison of the results in this work with that of some previously reported cycling performance of S/Se cathodes for Li-S batteries.

Material	Electrolyte	Current Density (A g^{-1})	Cycle number	Capacity retention (mAh g^{-1})	Ref.
Se_xS_{1-x}/pPAN	Carbonate	0.2	200	857.4	This work
	Ether	0.4	200	806.1	
	Ether	1	500	574.5	
SeS_x/cPAN	Carbonate	0.6	1200	780	1
pPAN/SeS_2	Carbonate	4	2000	633	2
$S_{0.87}Se_{0.13}$/CPAN	Carbonate	0.3	200	989	3
Se_xS_y/mesoporous carbon microsphere	Ether	0.5C	100	796.4	4
SeS_2/double-layered hollow carbon sphere	Carbonate	1C	900	610	5
S-rich $S_{1-x}Se_x$/C	Carbonate	1	500	910	6
Se_2S_5 confined in micro/mesoporous carbon	Ether	0.5C	100	430.2	7
Se_nS_{8-n} Molecules Confined in Nitrogen-Doped Mesoporous Carbons	Ether	0.25	200	780	8
$S_{22.2}Se$/Ketjenblack	HFE-based	1C	250	660	9
$NiCo_2S_4$@NC–SeS_2	Ether	1C	800	580	10
CMK-3/SeS_2@PDA	Ether	2	500	350	11
CoS_2@LRC/SeS_2	Ether	0.5	400	470	12
$S_{0.6}Se_{0.4}$@CNFs	Carbonate	1	1000	346	13
Co–N–C/SeS_2	Ether	0.2C	200	970.2	14
HMC@TiN/SeS_2	Ether	0.2C	200	690	15
S/Se@CB⊂NNH	Ether	0.2	500	915	16

Reference:

[1] C. Luo, Y. J. Zhu, Y. Wen, J. J. Wang, C. S. Wang, Carbonized Polyacrylonitrile-Stabilized SeS_x Cathodes for Long Cycle Life and High Power Density Lithium Ion Batteries, Adv. Funct. Mater. 24 (26) (2014) 4082-4089.

[2] Z. Li, J. T. Zhang, Y. Lu, X. W. Lou, A pyrolyzed polyacrylonitrile/selenium disulfide composite cathode with remarkable lithium and sodium storage performances, Sci. Adv. 4 (6) (2018) 1687.

[3] T. C. Zhu, Y. Pang, Y. G. Wang, C. X. Wang, Y. Y. Xia, $S_{0.87}Se_{0.13}$/CPAN composites as high capacity and stable cycling performance cathode for lithium sulfur battery, Electrochimica Acta 281 (2018) 789-795.

[4] Y. J. Wei, Y. Q. Tao, Z. K. Kong, L. Liu, J. T. Wang, W. N. Qiao, L. C. Ling, D. H. Long, Unique electrochemical behavior of heterocyclic selenium–sulfur cathode materials in ether-based electrolytes for rechargeable lithium batteries, Energy Storage Materials 5 (2016) 171-179.

[5] H. W. Zhang, L. Zhou, X. D. Huang, H. Song, C. Z. Yu, Encapsulation of selenium sulfide in double-layered hollow carbon spheres as advanced electrode material for lithium storage, Nano Research 9(12) (2016) 3725-3734.

[6] X. N. Li, J. W. Liang, K. L. Zhang, Z. G. Hou, W. Q. Zhang, Y. C. Zhu, Y. T. Qian, Amorphous S-rich $S_{1-x}Se_x$/C ($x \leqslant 0.1$) composites promise better lithium-sulfur batteries in a carbonate-based electrolyte, Energy Environ. Sci. 8(11) (2015) 3181-3186.

[7] G. L. Xu, T. Y. Ma, C. J. Sun, C. Lou, L. Cheng, Z. H. Chen, K. Amine, et al. Insight into the capacity fading mechanism of amorphous Se_2S_5 confined in micro/mesoporous carbon matrix in ether-based electrolytes, Nano letters 16(4) (2016) 2663-2673.

[8] F. G. Sun, H. Y. Cheng, J. Z. Chen, N. Zheng, Y. S. Li, J. L. Shi, Heteroatomic Se n S_{8-n} Molecules Confined in Nitrogen-Doped Mesoporous Carbons as Reversible Cathode Materials for High-Performance Lithium Batteries, ACS Nano 10(9) (2016) 8289-8298.

[9] G. L. Xu, H. Sun, C. Luo, L. Estevez, M. Hao, et al. Solid-State Lithium/Selenium-Sulfur Chemistry Enabled via a Robust Solid-Electrolyte Interphase, Adv. Energy Mater. 9(2) (2019) 1802235.

[10] B. S. Guo, T. T. Yang, W. Y. Du, Q. R. Ma, L. Z. Zhang, S. J. Bao, X. Y. Li, Y. M. Chen, M. W. Xu, Double-walled N-doped carbon@$NiCo_2S_4$ hollow capsules as SeS_2 hosts for advanced Li-SeS_2 batteries, J. Mater. Chem. A 7(19) (2019) 12276-12282.

[11] Z. Li, J. T. Zhang, H. B. Wu, X. W. Lou, An improved Li-SeS_2 battery with high energy density and long cycle life, Adv. Energy Mater. 7(15) (2017) 1700281.

[12] J. T. Zhang, Z. Li, X. W. Lou, A Freestanding Selenium Disulfide Cathode Based on Cobalt Disulfide-Decorated Multichannel Carbon Fibers with Enhanced Lithium Storage Performance, Angew. Chem. Int. Ed. 56(45) (2017) 14107-14112.

[13] Y. Yao, L. C. Zeng, S. H. Hu, Y. Jiang, B. B. Yuan, Y. Yu, Binding $S_{0.6}Se_{0.4}$ in 1D Carbon Nanofiber with C-S Bonding for High-Performance Flexible Li-S Batteries and Na-S Batteries, Small 13(19) (2017) 1603513.

[14] J. R. He, W. Q. Lv, Y. F. Chen, J. Xiong, K. C. Wen, C. Xu, W. L. Zhang, Y. R. Li, W. Qin, W. D. He, Direct impregnation of SeS_2 into a MOF-derived 3D nanoporous Co-N-C architecture towards superior rechargeable lithium batteries, J. Mater. Chem. A 6(22) (2018) 10466-10473.

[15] Z. Li, J. T. Zhang, B. Y. Guan, X. W. Lou, Mesoporous Carbon@titanium nitride hollow spheres as an efficient SeS_2 host for advanced Li-SeS_2 batteries, Angew. Chem. Int. Ed. 56(50) (2017) 16003-16007.

[16] T. Meng, Y. N. Liu, L. P. Li, J. H. Zhu, J. C. Gao, H. Zhang, L. Ma, C. M. Li, J. Jiang, Smart Merit Combination of Sulfur, Selenium and Electrode Engineering to Build Better Sustainable Li-Storage Batteries, ACS Sustainable Chem. Eng. 7(1) (2018) 802-809.